Structures of metallic clusters: Mono- and polyvalent metals

S. K. Lai[a)]
Complex Liquids Laboratory, Department of Physics, National Central University, Chung-li 320, Taiwan, Republic of China, Department of Physics, University of Waterloo, Waterloo, Ontario N2L 3G1, Canada, and Department of Physics, Tokyo Metropolitan University, Hachioji, Tokyo 192-0397, Japan

P. J. Hsu and K. L. Wu
Complex Liquids Laboratory, Department of Physics, National Central University, Chung-li 320, Taiwan, Republic of China

W. K. Liu
Department of Physics, University of Waterloo, Waterloo, Ontario N2L 3G1, Canada

M. Iwamatsu[b)]
Department of Physics, Tokyo Metropolitan University, Hachioji, Tokyo 192-0397, Japan

(Received 28 May 2002; accepted 23 September 2002)

We present detailed numerical results on the ground state structures of metallic clusters. The Gupta-type many-body potential is used to account for the interactions between atoms in the cluster. Both the genetic algorithm technique and the basin hopping method have been applied to search for the global energy minima of clusters. The excellent agreement found in both schemes for the global energy minima gives credence to the optimized energy values obtained. For four monovalent and one polyvalent metals studied in this work and within the accuracy of the energies presented here, we find that the global energy minima predicted by the basin hopping method are the same as those values obtained by the genetic algorithm. Our calculations for the ground state energies of alkali metallic clusters show regularities in the energy differences, and the cluster growth pattern manifested by this same group of clusters is generally icosahedral, which is quite different from the close-packed and decahedral preferentially exhibited by the tetravalent lead clusters. Considering the inherent disparities in the electronic properties and the bulk structures in these metals (body-centered cubic for alkali metals and face-centered cubic for the lead metal), it is not unreasonable to conjecture that the valence electrons do play a subtle role in the conformation of metallic clusters. [DOI: 10.1063/1.1521128]

I. INTRODUCTION

A theoretical calculation of finite-sized clusters composed of either metallic or nonmetallic atoms is fundamentally important since clusters lie in between the microscopic quantity, the atom, and the macroscopic quantity, the solid or liquid. In principle, one would be able to have a better understanding of the conformation of bulk crystalline structures if the atomic development of clusters can be followed as by progressively increasing the number of atoms until clusters have achieved sufficiently large size for the shifting over to their bulk counterparts to be realized. Such an ambitious idea has been a target of endeavor in several recent studies.[1–8] There are difficulties and ambiguities arising from this approach. First, it is hard to define with precision how large a cluster is to be called a bulk system. For example, cases exist[9,10] where clusters of extremely large size with 20 000 atoms or even 10^{14} atoms still show fivefold axes of symmetry. As a result, an attempt to extract bulk properties from clusters would require studying clusters with larger and larger size until the bulk characteristics show up. A considerable amount of computation is thus expected. Second, for a finite number of atoms, confined geometry will certainly make the calculation of the electronic energy state in a metallic cluster more difficult since the electron–ion interaction will not be weak per se and the usual low-order perturbation procedure for bulk systems is unjustified. Moreover many-body interactions and the surface effect are becoming more important in a finite system. Since a metal is characterized by the presence of valence electrons, two fundamental questions are as follows. What is the stable configuration of ions about which the valence electrons move? What role do valence electrons play in the conformation of a stable metallic cluster? It is the purpose of this work to address the former issue by calculating and analyzing the ground state configuration of metallic clusters. Hopefully the calculated results would yield an indirect probe to the questions. To this end, we study in particular the equilibrium structures of monovalent alkali metals whose electron density parameter r_s (defined by $4\pi r_s^3/3=\rho_e^{-1}$, ρ_e being the electron number density) lies in the range $4\lesssim r_s\lesssim 6$. We also study the tetravalent metal Pb whose electron density is about two to three times higher, i.e., $r_s\approx 2.3$. As regards the methodology, we employ two

a)Electronic mail: sklai@cliq.phy.ncu.edu.tw
b)Permanent address: Department of Physics, General Education Center, Musashi Institute of Technology, Setagaya-ku, Tokyo 158-8557, Japan.

widely used techniques to search for the global energy minima: the genetic algorithm[11,12] and the basin hopping Monte Carlo method.[13] Both methods have been evaluated in the literature showing various degree of promise.

II. COMPUTATIONAL DETAILS

In this section, we introduce the many-body potential and give documentary details of the genetic algorithm technique and basin hopping method. These ingredients are then applied to calculate the ground state geometries of the clusters of simple metals.

A. Gupta-type potential

As implied in Sec. I, it is difficult to construct from first principles a many-body potential for describing a finite-sized metallic cluster. We have therefore turned to an alternative analytic model, the *n*-body Gupta potential,[14] which was originally proposed for studying relaxation near surfaces and impurities in bulk transition metals.

The principal part of the *n*-body Gupta potential rests on the tight binding model originally proposed by Ducastelle[15] and Friedel.[16] The main idea consists of constructing a functional within the second moment approximation[17,18] which takes into account the essential band character of the metallic bond. Technically, we focus on the band structure term that is proportional to the effective bandwidth of the valence band given by the square root of the second moment of the local density of states. Inspired by the tight binding expression to represent the hopping integrals, the form of the functional is chosen to be[19]

$$V_d(i) = -\left[\sum_{j\neq i} \xi^2 \exp[-2q(r_{ij}/r_0 - 1)]\right]^{1/2}, \tag{1}$$

where r_0 is the equilibrium bulk interatomic distance taken to be the nearest-neighbor distance. To maintain stability of the system, a short-range repulsive force is added. Following Li *et al.*[18] and others,[15,16,20,21] the repulsive interaction is written

$$V_r(i) = \xi \sum_{j\neq i} \exp[-p(r_{ij}/r_0 - 1)], \tag{2}$$

where ξ and p, and those ζ and q given in Eq. (1) are parameters fitted to the local density approximation database.[22,23] The *n*-body Gupta-type potential now reads

$$E = \sum_i [V_r(i) + V_d(i)], \tag{3}$$

which is the many-body potential energy to be used in the following calculation of metallic clusters.

B. Method of genetic algorithm

We show in Fig. 1 the flow chart of our energy optimization procedure for the genetic algorithm strategy. Technically, the genetic algorithm is a search procedure inspired by the Darwinian evolution process.[24] Numerically it is an iterative, stochastic algorithm maintaining a population of individuals. Each individual (cluster), P_c, in the population consists of the Cartesian coordinates $P_c = (X_{c1}^1, X_{c2}^1, X_{c3}^1, X_{c1}^2, X_{c2}^2, X_{c3}^2, \ldots, X_{c1}^n, X_{c2}^n, X_{c3}^n)$ of n atoms. Thus, the cluster P_c of n atoms in three dimension can be expressed in one dimension as

$$P_c = (X_{c1}^1, X_{c2}^1, X_{c3}^1, X_{c1}^2, X_{c2}^2, X_{c3}^2, \ldots, X_{c1}^n, X_{c2}^n, X_{c3}^n) = (X_c^1, X_c^2, X_c^3, \ldots, X_c^{3n}).$$

The individual whose variables $\{\mathbf{X}\}$ are the Cartesian coordinates (playing the role of genes) has been encoded in the form of a string much like a chromosome. Each string represents a possible solution of the problem. A total of twenty individuals, $N=20$, i.e., (P_c, $c=1,\ldots,20$), were chosen for this work. Now, given the individuals $(P_1, P_2, \ldots, P_{20})$, we use the above-introduced Gupta-type potential to calculate the potential energy, $V_c = V(P_c)$, $c=1,2,\ldots,20$ for all individuals and determine their local minima by the conjugate gradient minimization, using the L-BFGS method.[25] Then, as shown in Fig. 1, an evaluation of the ''fitness'' of each individual is performed. The fitness of the ith individual F_i is designated by

$$F_i = (V_{\max} - V_i)/(V_{\max} - V_{\min}), \tag{4}$$

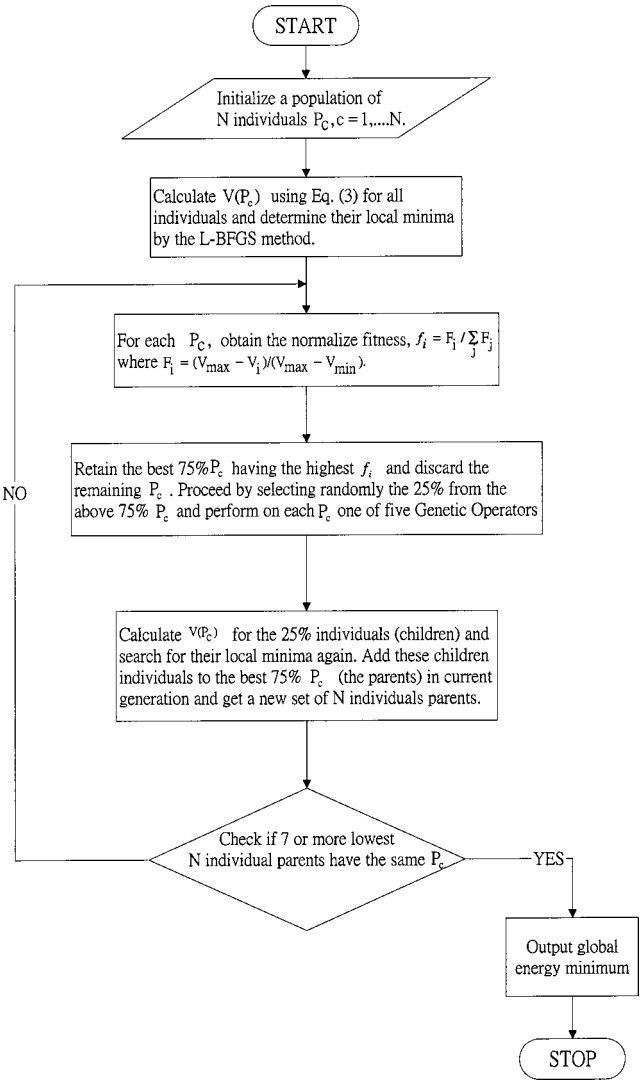

FIG. 1. Flow chart for the genetic algorithm method.

where $V_{\max}(V_{\min})$ is the maximum (minimum) of $\{V_{c=1}, V_{c=2}, \ldots, V_{c=20}\}$. The normalized fitness f_i is evaluated as

$$f_i = \frac{F_i}{\Sigma_{j=1}^{20} F_j}. \tag{5}$$

Having determined the fitness for all individuals, the statistic is used in the preparation of next generation (the ''children''). In this work, we retain the best 75% of the individuals (the ones with the highest fitness) in the current generation, i.e., these individuals are passed intact to the next generation. The remaining 25% of the individuals in the next generation are selected randomly from the best 75% mentioned previously and subject to one of the five genetic operators:

1. Inversion;
2. Arithmetic mean;
3. Geometric mean; (6)
4. N-point crossover;
5. 2-point crossover.

The meaning of each genetic operator is explained in the work of Niesse and Mayne[12] (see also Refs. 11, 26, and 27 to which we refer the interested readers for details). Basically what the genetic operators do is either to transform an individual into a different individual or to ''breed'' one child from two parents. After several trials, we have stipulated, somewhat judiciously, the weighting of genetic operators 1–5 in the ratio of 5:1:1:5:5. In this way the population size is always kept constant.

After the twenty parents (fifteen passing intact plus five newly generated by use of genetic operators) are generated, we proceed to again locate their local minima. The above-described procedure is repeated until the population contains at least 7 best fitted structures whose potential energies remain unchanged. We should emphasize at this point that we have written our computer code in a MPI parallelized form because the minimization runs of the initial twenty parents and the subsequent generation of 5 children are independent. Efficient use of the CPU is therefore achieved. In addition to parallelizing the code, we have also tried to reduce the computing time by incorporating a seeding procedure.[12] To ensure the reliability of the latter procedure, we have carried out similar calculations also for clusters without seeding. Except for the notably long computing time for the latter, both procedures yield the same global minimum energy.

C. Basin hopping method

In this approach we have been guided by the works of Wales and Doye[28] and of Li and Scheraga.[29] The basic idea of the method rests on monitoring an initial potential energy surface (PES) $V(\mathbf{r}_1, \mathbf{r}_2, \ldots, \mathbf{r}_n) \equiv V(\mathbf{X})$ of n atoms which is transformed so that the resulting PES does not change the global minimum or the relative energies of local minima. In other words, the PES of $V(\mathbf{X})$ is deformed into a multidimensional staircase topography $\tilde{V}(\mathbf{X})$ given by

$$\tilde{V}(\mathbf{X}) = \min[V(\mathbf{X})], \tag{7}$$

where the min represents a local energy minimization starting from the coordinates $\{\mathbf{r}_1, \mathbf{r}_2, \ldots, \mathbf{r}_n\}$ of n atoms. Technically the numerical procedure runs as follows. For a cluster of n atoms, we randomly generate an atomic configuration that is confined inside a sphere of radius $R_d = r_0[1 + (3n/4\pi\sqrt{2})^{1/3}]$, r_0 being the nearest-neighbor distance, whose origin is located at the center-of-mass of the cluster. The confinement of n atoms within R_d is done to prevent the whole cluster from evaporating. We next pinpoint that particular atom whose location $r_{\max}$ from the origin is farthest compared with others. Given the configuration of a cluster, we can calculate the potential energy by Eq. (7). Following Wales and Doye,[28] we apply a canonical Monte Carlo simulation to search for the above-described deformed PES. In Fig. 2 we depict schematically the flow chart of the method. In connection with this flow chart, we comment further on the following technical points.

a. Angular move and random displacement: Given the configuration of an n-atoms cluster, the local minimum is determined as follows. First, we apply angular moves and random displacements to the n-atoms cluster. We call these processes a *step*. For an additive potential, it is easy to write down the energy as

$$E = 1/2 \sum_{i=1}^{n} V(i),$$

where $V(i)$ refers to the potential of the ith atom due to its interaction with all the other atoms at $(\mathbf{r}_1, \ldots, \mathbf{r}_{i-1}, \mathbf{r}_{i+1}, \ldots, \mathbf{r}_n)$. Among the $V(i)$, $i = 1,...,n$, we sort out the two particles with the lowest, V_l, and the highest, V_h, energies. If $V_h > \nu V_l$ where the constant ν satisfies $0 < \nu < 1$, we move the V_h atom to the surface of $r_{\max}$ and displace all others by a random number δ that lies in the range $0 < \delta < 1$.

b. Seeding: To reduce computing time, we use the existing set of coordinates for the initial configuration. This procedure is applied in parallel with a randomly generated configuration (no seeding) to check the reliability of our calculated results.

c. Limited BFGS algorithm: This is one of the variable metric methods and is an efficient approach in searching the local minimum.[25] The basic idea lies in the usual Monte Carlo moves where we apply the root-mean-square gradient to determine how far the moves are to be accepted during the iterations of the L-BFGS. Initially the convergence criterion needs not be very tight, thus saving a lot of computing time. In the final stage the L-BFGS is carried out again now using a tightly convergence criterion.

d. Quenching: Based on Markov's process, the Monte Carlo simulation starts by going downhill, which leads to a local (but not necessarily a global) minimum. Statistically the system must obey a Boltzmann probability distribution $P(E)$ in thermal equilibrium at temperature T for all different energy states E that satisfies

$$P(E) \sim e^{-\Delta E/T}.$$

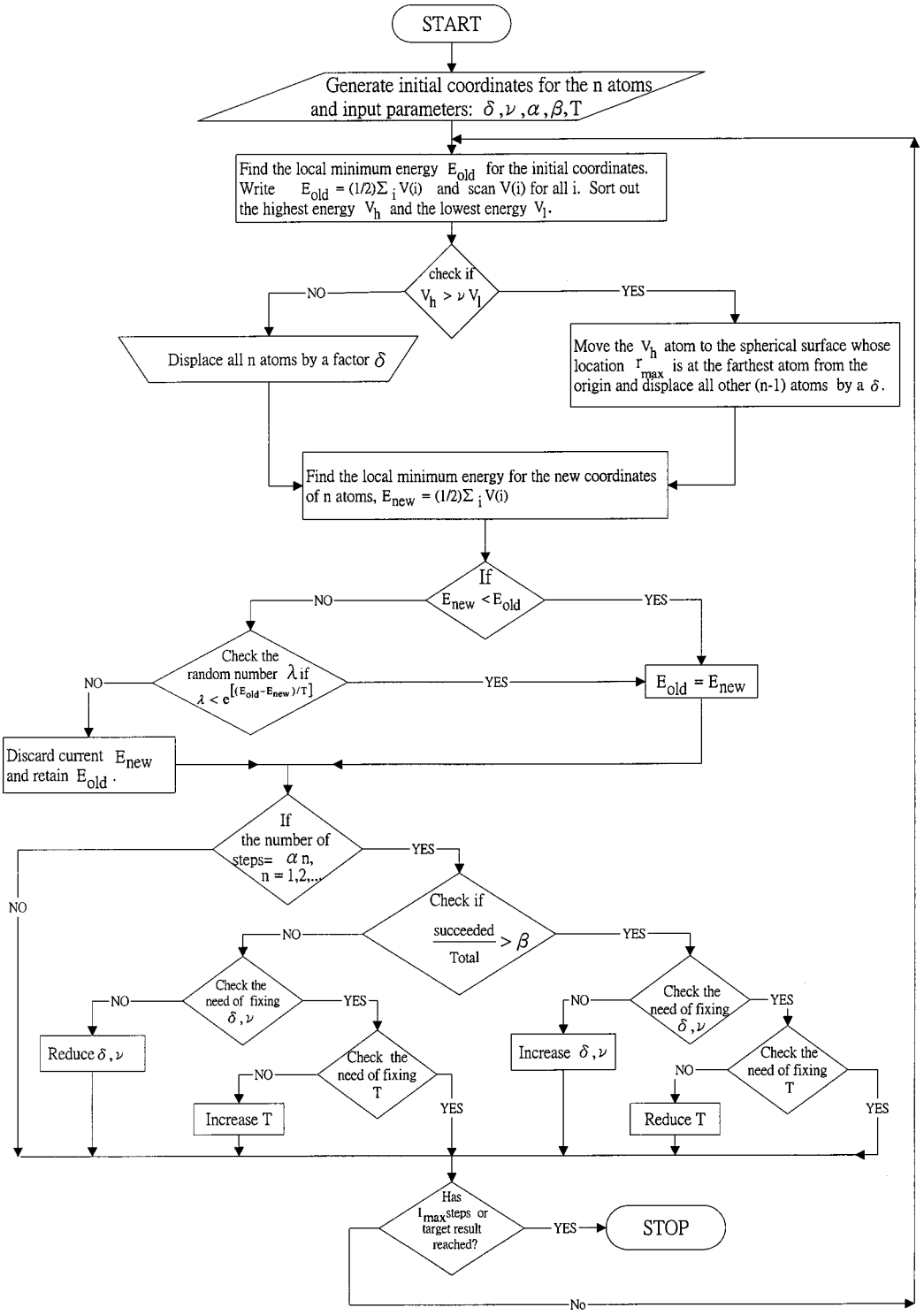

FIG. 2. Flow chart for the basin hopping method.

Although the original Monte Carlo method is used at a constant T, in the basin hopping method we may still increase or decrease the temperature in the course of taking steps. For example, supposing $\Delta E>0$, which only happens when the search for the energy landscape is difficult, we may vary the temperature to find the range of energy states so that the latter difficulty can be resolved. In general, after a few intervals of steps, the temperature is lowered slowly, which corresponds to narrowing the range of energy states. Note that the parameters $\alpha>0$ and $0<\beta<1$ in the flow chart play the role of acceptance ratio check. Also, in the present work, T is either changed or fixed at 0.8 in each Monte Carlo step. Specifically, we set the acceptance ratio, δ and ν, to the values 0.5, 0.36, and 0.4, respectively. We terminate the calculation when the total number of steps $I_{\max}$ has reached 5000. Alternatively, the program can also be used for the case where a target potential is available as a termination criterion. It should be emphasized that the nature of the trans-

TABLE I. Gupta-type potential parameters ξ, ζ, p, q, and r_0 for four alkali metals and the polyvalent metal Pb. The parameters for the alkali metals and Pb are taken from Li *et al.* (Ref. 18) and Cleri and Rosato (Ref. 17), respectively.

Metal	ξ (eV)	ζ (eV)	p	q	r_0 (a.u.)
Na	0.015 96	0.291 14	10.130 94	1.302 18	6.9921
K	0.020 54	0.262 59	10.58	1.34	8.253
Rb	0.019 46	0.246 54	10.48	1.4	8.81
Cs	0.020 54	0.242 18	9.62	1.45	9.44
Pb	0.098 00	0.914 00	9.576	3.648	6.6157

formed PES permits relatively large step sizes to be taken. Further details of the method is schematically depicted in Fig. 2.

III. NUMERICAL RESULTS

We present results for the monovalent alkali metals and the polyvalent metal lead.

A. Monovalent metals: Na, K, Rb, and Cs

Among the sp-type simple metals that have been studied in the literature, the alkali metals are often chosen as prototype systems for detailed investigation. These metals are characterized by their relatively simple electronic structures, making theoretical analysis easier. We first applied the two algorithms mentioned earlier to four alkali metals using the Gupta-type potential function whose parameters are taken from Li *et al.*[18] We should emphasize that in the rigorous calculations of Li *et al.* using local density approximation, the attractive interaction between atoms has been calculated by summing over neighbors within 12 coordination shells in a bulk crystal. The potential function parameters, collected in Table I, are thus based on the first-principles results instead of fitting them to experimental quantities as done for some transition metals.[17] For all of four alkali metals, we consider clusters in the size range $3 \leqslant n \leqslant 56$. Unless explicitly specified, we shall use the notation $\mathfrak{I}_n$ for a general n-atom neutral cluster; in the present case $\mathfrak{I}$ stands for Na, K, Rb, or Cs.

Let us begin by presenting in Table II the global energy minima for the alkali-metal clusters determined using the approach of genetic algorithm and the basin-hopping method. For all of four alkali metals the calculated n-atom binding energies $E(n)$ [see Eq. (3)] in both schemes are the same, thus lending credence to the structure of the $\mathfrak{I}_n$ obtained. Employing $E(n)$, we plot in Figs. 3(a)–3(d), respectively, for Na, K, Rb, and Cs, the energy difference $\Delta E(n) = E(n) - E_{\mathfrak{I}}(n)$ and the second energy difference $\Delta_2 E(n) = [E(n+1) - E(n)] - [E(n) - E(n-1)]$, where

$$E_{\mathfrak{I}}(n) = A + Bn^{1/3} + C(n^{1/3})^2 + D(n^{1/3})^3. \quad (8)$$

Equation (8) is applied to each alkali metal with the coefficients A, B, C, and D, given in Table III, determined by a least-squares fit to the global energy minima $E(n)$, $3 \leqslant n \leqslant 57$. Note that the expansion of $E_{\mathfrak{I}}(n)$ as a power of $n^{1/3}$ can be given physical significance. Since the size of the cluster is proportional to n, the coefficients A, B, C, and D represent contributions of the vertex, edge, surface, and bulk to the cluster cohesive energy, respectively. The $\Delta_2 E(n)$ measures the stability of an n-atom structure with respect to its neighboring sizes and has the value zero if $\mathfrak{I}_n$ is not relatively more stable than its neighbors. It has been found in the literature that $\Delta_2 E(n)$ correlates closely with the measured mass spectra.[30] The implication of the calculated energy difference and the optimized ground-state geometries for this group of metallic clusters can be summarized as follows.

(a) Referring to Figs. 3(a)–3(d), it can be seen that the complete Mackay icosahedra $\mathfrak{I}_{13}$ and $\mathfrak{I}_{55}$ stand out as the most stable for all four alkali metals. A sequence of other stable structures are $\mathfrak{I}_{19}$, $\mathfrak{I}_{23}$, $\mathfrak{I}_{26}$, $\mathfrak{I}_{29}$, $\mathfrak{I}_{32}$, and $\mathfrak{I}_{34}$. For these stable clusters the structures for all of four alkali metals are identical. We include them in Figs. 4(a)–4(d) where, in addition, we depict separately for Na, K, Rb, and Cs all other clusters in the size range $3 \leqslant n \leqslant 56$. Interestingly, there is regularity in the growth of these stable structures: the $\mathfrak{I}_{13}$ is an icosahedron, the 19-atom double icosahedron is formed by joining $\mathfrak{I}_{13}$ with a pentagonal bipyramid $\mathfrak{I}_7$ in which both share one common apex. Upon moving from $\mathfrak{I}_{19}$ to other stable clusters, a single capped pentagonal pyramid is attached to the central belt leading first to $\mathfrak{I}_{23}$, or multiple capped pentagonal pyramids are fused and attached jointly to the side of $\mathfrak{I}_{19}$ leading succeedingly to larger stable sizes for $n = 26$, 29, 32, and 34. It is perhaps interesting to notice the trend of these stable structures, despite the fact that bulk electronic densities of alkali metals vary somewhat from Na to Cs.

(b) Based on the compatible results given in Table II for the global energy minima, we now discuss in more detail the equilibrium structures at $T = 0$ K. In the first place, we note that the clusters $\mathfrak{I}_3$–$\mathfrak{I}_8$ are the same for all four alkali metals. Initially the cluster takes on a planar $\mathfrak{I}_3$, assumes a regular triangular pyramid $\mathfrak{I}_4$, grows into a triangular bipyramid $\mathfrak{I}_5$, turns to a tetrahedral bipyramid (octahedron) $\mathfrak{I}_6$, and then develops from a pentagonal bipyramid $\mathfrak{I}_7$ into a dodecaheron $\mathfrak{I}_8$. These metallic clusters are displayed in Figs. 4(a)–4(d), respectively, for the Na, K, Rb, and Cs. Note that the pentagonal bipyramid $\mathfrak{I}_7$ and tetrahedral pyramid $\mathfrak{I}_4$ are central motifs in subsequent growth of larger clusters.

(c) The case $\mathfrak{I}_9$ deserves due attention. For the three alkali metals, Na, K, and Cs, their clusters $\mathfrak{I}_9$ have the regular tetrahedral bipyramid with one apex replaced by two atoms forming the common edge of two regular tetrahedral pyramids. The cluster Rb_9, however, takes on an entirely different structure. It has a C_{2v} symmetry consisting of a Rb_7 pentagonal bipyramid with two more atoms placed at adjacent sites that form an equilateral triangle with one common apex, in addition to each of the adjacent atoms joining two atoms on the pentagonal ring of Rb_7 to form equilateral triangles. The same $\mathfrak{I}_9$ structure is previously predicted for the Lennard-Jones as well as Sutton–Chen 10-8 potentials.[28] For the Rb metal, Rb_9 is the starting configuration for the cluster to grow by adding one atom at a time to the aforementioned two adjacent atoms until it evolves into a 13-atom icosahedron. In contrast, the clusters $\mathfrak{I}_{10}$–$\mathfrak{I}_{12}$ of the other three alkali metals, Na, K, and Cs, all exhibit the same structures as Rb; their growth pattern into the 13-atom icosahedron thus begins with $\mathfrak{I}_{10}$. Figures 4(a)–4(d) depict these symmetries.

(d) Coming to $\mathfrak{I}_{14}$–$\mathfrak{I}_{19}$, the cluster size $n = 15$ shows an

TABLE II. Global energy minima, in units of eV, for metallic clusters (a) sodium, (b) potassium, (c) rubidium, and (d) caesium. Within the accuracy of the energy values listed, both the basin hopping (BH) method and the genetic algorithm (GA) are the same.

(a)	*n*	3	4	5	6	7	8	9	10
	BH/GA	−1.159 775	−1.838 112	−2.512 921	−3.268 090	−3.980 169	−4.718 026	−5.468 145	−6.249 708
	n	11	12	13	14	15	16	17	18
	BH/GA	−7.045 767	−7.929 663	−8.886 274	−9.601 137	−10.436 000	−11.232 841	−12.046 461	−12.913 720
	n	19	20	21	22	23	24	25	26
	BH/GA	−13.859 077	−14.681 809	−15.502 668	−16.382 753	−17.337 906	−18.160 810	−19.043 948	−20.006 273
	n	27	28	29	30	31	32	33	34
	BH/GA	−20.829 107	−21.730 297	−22.663 656	−23.489 360	−24.369 877	−25.321 450	−26.203 889	−27.164 454
	n	35	36	37	38	39	40	41	42
	BH/GA	−28.052 346	−28.921 899	−29.852 456	−30.797 997	−31.716 489	−32.596 053	−33.518 644	−34.434 080
	n	43	44	45	46	47	48	49	50
	BH/GA	−35.355 908	−36.272 608	−37.184 443	−38.158 884	−39.073 434	−40.039 811	−41.030 280	−42.018 288
	n	51	52	53	54	55	56	57	
	BH/GA	−43.008 822	−43.999 192	−44.989 427	−45.982 190	−46.977 660	−47.814 265	−48.695 945	
(b)	*n*	3	4	5	6	7	8	9	10
	BH/GA	−0.992 259	−1.573 407	−2.148 020	−2.789 214	−3.394 135	−4.015 074	−4.645 523	−5.311 416
	n	11	12	13	14	15	16	17	18
	BH/GA	−5.982 128	−6.727 781	−7.539 342	−8.136 182	−8.825 738	−9.492 494	−10.172 982	−10.913 606
	n	19	20	21	22	23	24	25	26
	BH/GA	−11.712 693	−12.398 368	−13.081 451	−13.817 220	−14.619 481	−15.303 643	−16.037 740	−16.842 136
	n	27	28	29	30	31	32	33	34
	BH/GA	−17.526 245	−18.281 539	−19.054 481	−19.740 179	−20.472 589	−21.264 667	−21.991 011	−22.798 404
	n	35	36	37	38	39	40	41	42
	BH/GA	−23.541 792	−24.266 168	−25.038 222	−25.845 384	−26.612 329	−27.343 734	−28.089 804	−28.859 860
	n	43	44	45	46	47	48	49	50
	BH/GA	−29.616 661	−30.385 711	−31.166 266	−31.988 788	−32.738 720	−33.547 647	−34.369 846	−35.181 512
	n	51	52	53	54	55	56	57	
	BH/GA	−36.010 242	−36.838 775	−37.667 114	−38.497 012	−39.328 556	−40.015 908	−40.726 052	
(c)	*n*	3	4	5	6	7	8	9	10
	BH/GA	−0.931 695	−1.474 630	−2.010 000	−2.606 428	−3.168 620	−3.744 182	−4.327 892	−4.945 860
	n	11	12	13	14	15	16	17	18
	BH/GA	−5.566 297	−6.255 998	−7.007 640	−7.558 542	−8.195 293	−8.811 605	−9.439 122	−10.122 184
	n	19	20	21	22	23	24	25	26
	BH/GA	−10.861 670	−11.493 101	−12.121 418	−12.799 584	−13.539 970	−14.169 202	−14.844 147	−15.584 940
	n	27	28	29	30	31	32	33	34
	BH/GA	−16.214 241	−16.912 560	−17.620 608	−18.251 314	−18.926 464	−19.653 573	−20.320 168	−21.065 132
	n	35	36	37	38	39	40	41	42
	BH/GA	−21.749 681	−22.416 455	−23.126 047	−23.869 250	−24.577 403	−25.250 774	−25.931 521	−26.642 461
	n	43	44	45	46	47	48	49	50
	BH/GA	−27.340 982	−28.044 309	−28.763 569	−29.521 178	−30.208 138	−30.950 981	−31.708 139	−32.446 678
	n	51	52	53	54	55	56	57	
	BH/GA	−33.208 915	−33.970 960	−34.732 814	−35.495 737	−36.259 809	−36.889 426	−37.539 878	
(d)	*n*	3	4	5	6	7	8	9	10
	BH/GA	−0.908 720	−1.431 490	−1.946 325	−2.519 216	−3.057 637	−3.610 119	−4.169 386	−4.757 794
	n	11	12	13	14	15	16	17	18
	BH/GA	−5.349 794	−6.007 189	−6.722 435	−7.249 200	−7.864 235	−8.451 273	−9.050 886	−9.692 558
	n	19	20	21	22	23	24	25	26
	BH/GA	−10.396 648	−10.998 239	−11.597 350	−12.241 653	−12.945 895	−13.544 953	−14.186 717	−14.890 823
	n	27	28	29	30	31	32	33	34
	BH/GA	−15.489 924	−16.157 686	−16.827 863	−17.429 012	−18.075 242	−18.762 272	−19.399 238	−20.106 494
	n	35	36	37	38	39	40	41	42
	BH/GA	−20.755 787	−21.390 264	−22.065 504	−22.758 963	−23.437 182	−24.078 990	−24.729 772	−25.405 425
	n	43	44	45	46	47	48	49	50
	BH/GA	−26.056 743	−26.737 652	−27.406 188	−28.123 848	−28.776 360	−29.479 340	−30.196 574	−30.895 293
	N	51	52	53	54	55	56	57	
	BH/GA	−31.616 817	−32.338 166	−33.059 342	−33.781 209	−34.503 854	−35.102 995	−35.731 711	

unique symmetry of assuming the hexagonal bipyramid similar to that of the Sutton–Chen 9-6 potential.[13] Interestingly, all four alkali metals take on this structure. The cases $\mathfrak{I}_{16}$ and $\mathfrak{I}_{17}$ vary somewhat among the four metals. They do, however, reveal a trace of common features. These clusters are formed by protruding either the capped pentagonal pyramid or the tetrahedral pyramid that appears with different relative orientations in the structure. With the exception of K_{17} displaying a disordered structure, the clusters K_{16}, Rb_{16}, and Rb_{17} basically evolve from a 13-atom icosahedron with atoms placed at sites that join the ring of $\mathfrak{I}_7$ to form equilateral triangles, whereas for the Na_{16}, Na_{17}, Cs_{16}, and Cs_{17} the

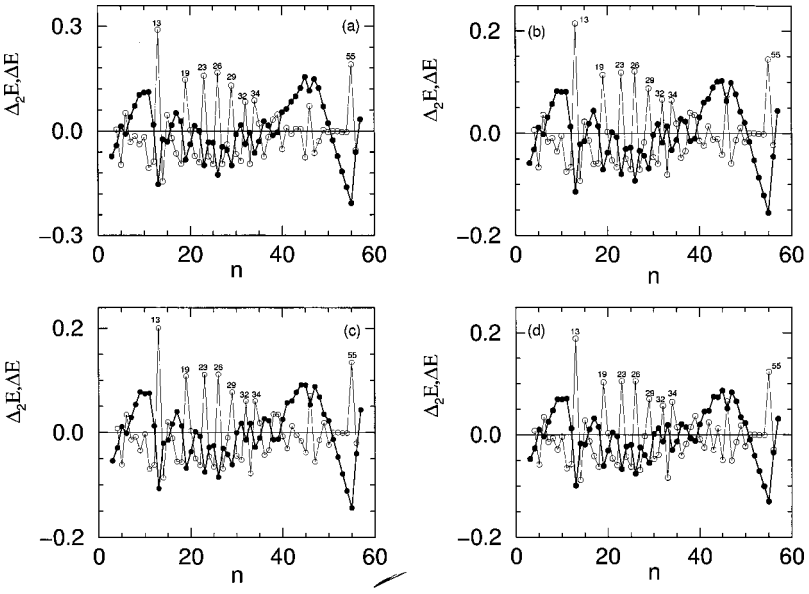

FIG. 3. The energy difference $\Delta E(n)$, denoted by closed circles, and the second energy difference $\Delta_2 E(n)$, denoted by open circles, for the alkali metallic clusters (a) Na, (b) K, (c) Rb, and (d) Cs.

evolution of clusters continues from the cluster structure $\mathfrak{I}_{15}$ with one of the vertex atoms removed and is replaced by two atoms becoming an edge in $\mathfrak{I}_{16}$, or three atoms forming an equilateral triangle in $\mathfrak{I}_{17}$. Geometrically, the original seven-coordinate hexagonal face of $\mathfrak{I}_{16}$ changes to two pentagonal pyramids fused together by sharing three edge coordinates, whereas for $\mathfrak{I}_{17}$, the hexagonal face is replaced by a pentagonal pyramid with three of the edges forming equilateral triangles with atoms at the ring. The clusters $\mathfrak{I}_{14}$ and $\mathfrak{I}_{18}$ are identical for all four alkali metals; the former is the 13-atom icosahedron with an extra atom placed at the site that formed a regular triangular pyramid, and the latter is the double icosahedron with one missing apex. All of four alkali metals recover the double icosahedron at $n=19$. The equilibrium structures of $\mathfrak{I}_{14}$–$\mathfrak{I}_{19}$ at $T=0$ K are again shown in Figs. 4(a)–4(d).

(e) There is systematic change in the growth of clusters $\mathfrak{I}_{20}$–$\mathfrak{I}_{40}$. It can be visualized by focusing on a seeding unit, the double icosahedron $\mathfrak{I}_{19}$, and observing how the cluster develops. Regularly the atoms occupy sites which tend to form a tetrahedral pyramid, pentagonal pyramid, or fused pentagonal pyramids with two shared edge atoms. The growth continues until the double icosahedron is surrounded on the cluster surface by pentagonal pyramids with different relative orientations. All four alkali metals follow this general pattern. Among clusters in this size range, we should mention two particular cases. First, Cs_{21} is of special interest.

TABLE III. Numerical values for the coefficients of the energy $E_{\mathfrak{I}}(n)=A+Bn^{1/3}+C(n^{1/3})^2+D(n^{1/3})^3$ appeared in the energy difference $\Delta E=E(n)-E_{\mathfrak{I}}(n)$ for the four alkali and the lead metallic clusters.

Metal	A	B	C	D
Na	2.112 39	−2.792 52	2.249 38	−1.287 81
K	2.028 23	−2.569 45	1.903 52	−1.071 98
Rb	1.890 61	−2.347 69	1.706 73	−0.977 49
Cs	1.664 34	−2.025 31	1.503 02	−0.910 42
Pb	1.800 99	−1.573 84	1.172 27	−2.083 95

This cluster differs from the $\mathfrak{I}_{21}$ of other alkali metals in that it is formed by adding six-coordinate atoms (pentagonal pyramid) to Cs_{15}. Second, $\mathfrak{I}_{36}$ and $\mathfrak{I}_{38}$ are somewhat exceptional. The former is the truncated octahedron $\mathfrak{I}_{38}$ with two less atoms but the cluster surfaces are distorted. The latter, on the other hand, shows discernible differences for the four metals; the K and Rb display typical truncated octahedrons with atoms occupying hexagonal and *square* faces, whereas for the Na and Cs their truncated octahedrons have hexagonal and *rhombus* faces [see Figs. 4(a)–4(d) for these structural disparities]. In connection to $\mathfrak{I}_{38}$, it is worthwhile remarking that our Na_{38} result agrees with that reported earlier by Calvo and Spiegelmann (Fig. 2 in Ref. 4).

(f) We now comment on the development of clusters for $n=41$–56. As Figs. 3(a)–3(d) show, $\mathfrak{I}_{55}$ is a distinctly stable cluster irrespective of the alkali metals. For the other $\mathfrak{I}_n$, the geometries for Na_{44}, Na_{45}, and Na_{49} are somewhat unique in comparison with K_{44}, Rb_{44}, and Cs_{44}, which all show identical structures. Also, we check that all of the remaining clusters for the four alkali metals in this size range evolve in the same way, i.e., $\mathfrak{I}_n$ approaches regularly the icosahedron symmetry with capped atoms occupying sites that form motifs $\mathfrak{I}_7$ or the pentagonal pyramid. The trend of cluster evolution is heading toward the complete Mackay icosahedron $\mathfrak{I}_{55}$. The readers can see the regular change in structures in Figs. 4(a)–4(d).

(g) For the cases of sodium and caesium, there are several more recent theoretical studies[4,18,31] as well as earlier representative simulation data[32] available for comparison. First, we check our calculated ground state clusters by comparing Na_8, Na_9, Na_{13}, Na_{20}, Na_{38}, Na_{40}, and Na_{55} with those Na_n reported by Calvo and Spiegelmann,[4] who applied the same Gupta-type potential and basin hopping method as we do. Except for the Na_8, for which our calculation shows a D_{2d} symmetry, our predicted Na_n agree with those obtained by these authors. Our calculated Na_8 is, however, in agreement with the Na_8 obtained independently by Röthlisberger and Andreoni[32] using the Car–Parrinello simulation

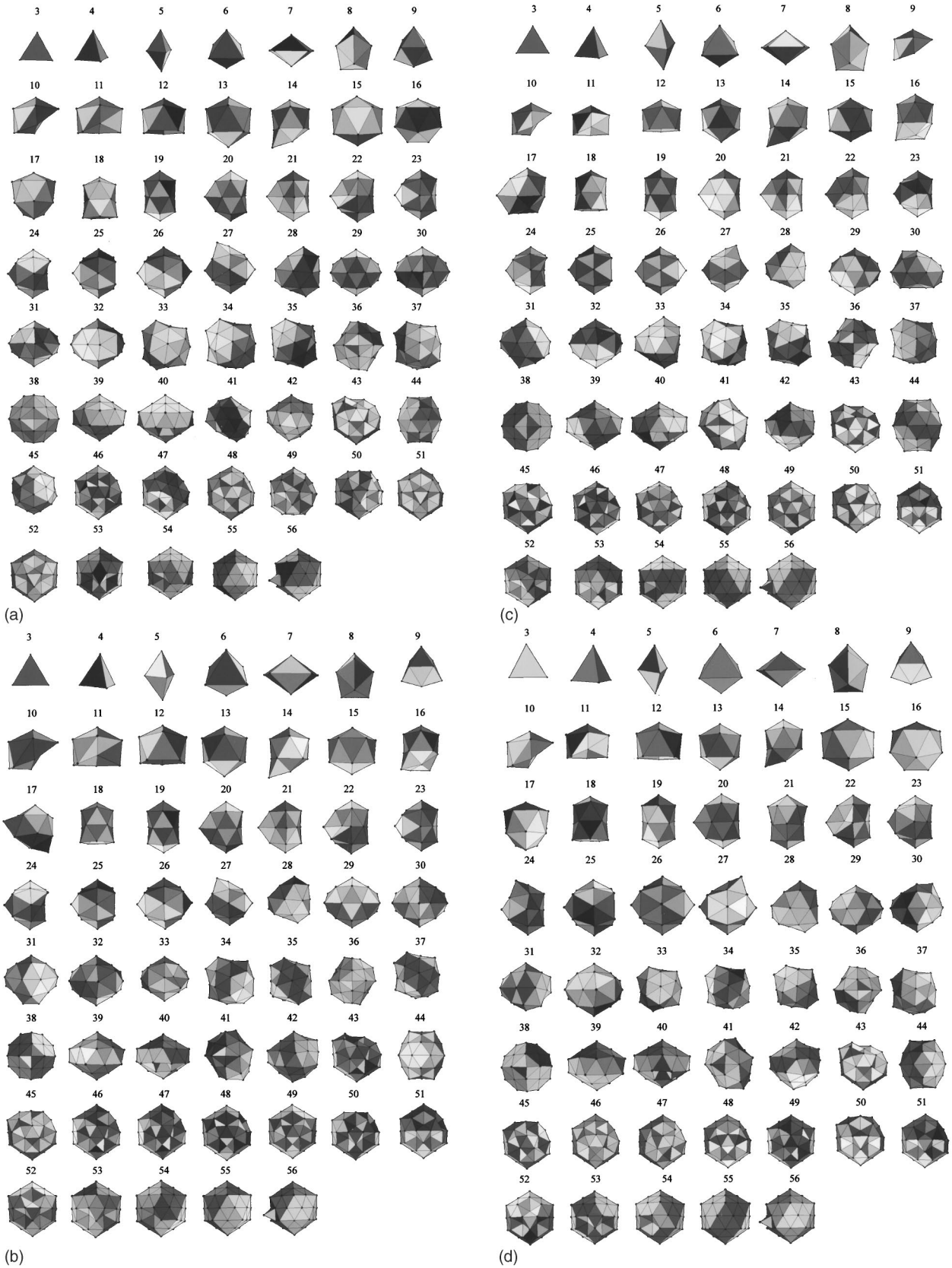

FIG. 4. Structures of the global energy minima for the alkali metallic clusters (a) Na, (b) K, (c) Rb, and (d) Cs calculated using Eqs. (1)–(3) with parameters documented in Table I. Within the accuracy of the energies presented here, the genetic algorithm and the basin hopping methods yield the same results.

method and by Aguodo *et al.*[31] applying the orbital free molecular dynamics simulation. Note that while our calculations applying the genetic algorithm and basin hopping method yield a point group symmetry D_{2d} for Na_8, it differs from the T_d symmetry predicted by the self-consistent field-configuration interaction calculations.[33,34] We should perhaps mention also that in addition to Na_8, our global minima for Na_{18} and Na_{20} are similar to those of Röthlisberger and

TABLE IV. Global energy minima, in units of eV, for the metallic cluster lead. Within the accuracy of the energy values listed, both the basin hopping (BH) method and the genetic algorithm (GA) are the same.

n	3	4	5	6	7	8	9	10
BH/GA	−4.231 623	−6.099 713	−7.886 887	−9.755 691	−11.556 399	−13.327 552	−15.144 569	−16.964 624
n	11	12	13	14	15	16	17	18
BH/GA	−18.763 845	−20.578 513	−22.582 268	−24.314 589	−26.251 715	−28.118 744	−29.970 807	−31.807 535
n	19	20	21	22	23	24	25	26
BH/GA	−33.630 068	−35.455 113	−37.331 152	−39.259 153	−41.158 168	−43.011 298	−44.836 232	−46.711 165
n	27	28	29	30	31	32	33	34
BH/GA	−48.618 275	−50.525 085	−52.420 239	−54.337 044	−56.148 061	−58.061 382	−59.923 960	−61.841 131
n	35	36	37	38	39	40	41	42
BH/GA	−63.721 029	−65.627 949	−67.555 414	−69.488 671	−71.356 501	−73.262 765	−75.112 815	−77.023 172
n	43	44	45	46	47	48	49	50
BH/GA	−78.929 624	−80.861 957	−82.746 569	−84.666 163	−86.561 577	−88.486 882	−90.376 393	−92.273 039
n	51	52	53	54	55	56	57	
BH/GA	−94.158 338	−96.110 031	−98.050 792	−99.932 185	−101.835 278	−103.741 499	−105.662 759	

Andreoni,[32] although disagreement remains for Na_6, Na_9, and Na_{13}.

Coming to the caesium clusters, we compare our results with those carried out by Li *et al.*,[18] who determined the Gupta-type potential parameters given in Table I in the local density approximation. These authors applied the dynamical optimization of the minimum energy to study cluster structures of four alkali metals and reported only selected clusters of Cs_8, Cs_9, Cs_{10}, Cs_{11}, Cs_{13}, and Cs_{20}. Since they only published those Cs_n that appear different from those for Na_n obtained by Röthlisberger and Andreoni,[32] it is not clear if the displayed Cs_n given by them correspond to the lowest energy minima. However, for the set of Cs_n given in Figs. 2 and 3 of Ref. 18 of their work, our calculated Cs_n is seen to agree with the Cs_{20} shown there as a lowest energy minimum.

B. Tetravalent metal: Pb

In analogy with the alkali metals, in the following we present our results of computations for Pb_n for the range of cluster sizes $3 \leqslant n \leqslant 56$. Before analyzing these clusters, two main points regarding the input parameters and the methodology used in the numerical works are in order. First, in contrast to the alkali metals, the Gupta potential parameters for Pb, given in Table I, have been taken from Cleri and Rosato,[17] who determined them by fitting to experimental bulk values. Second, despite the excellent agreement in binding energies obtained using both the genetic algorithm technique and the basin hopping method for alkali metals, we continue calculating these values for Pb using both schemes. Table IV lists these n-atom binding energies from which we obtain $\Delta E(n)$ and $\Delta_2 E(n)$. It can be seen from Fig. 5 that clusters Pb_{13}, Pb_{23}, Pb_{30}, Pb_{38}, and Pb_{53} are relatively more stable than others. With the exception of Pb_{13} and Pb_{38}, the occurrence of these stable clusters in the $\Delta E(n)$ and $\Delta_2 E(n)$ plots are seen to be quite different from those for the alkali metals, and accordingly their cluster symmetries are expected to be different also. Figure 6 shows the ground-state structures for the range of cluster sizes considered here. We note three general features.

(1) Up to Pb_{13}, the ground-state geometries of metallic clusters Pb and Rb are the same. This is due to our finding for Rb_9 assuming a C_{2v} structure [recall Sec. III A(c)]. The Pb_{14} has one atom less of the seven-coordinate vertices and is similar to the $\mathfrak{I}_{14}$ of Sutton–Chen 10-8 potential.[13] Interestingly, all four alkali metals and Pb metal show the same symmetry for $\mathfrak{I}_{15}$. The 15-atom cluster simply recovers the missing atom at the vertex of the cluster Pb_{14} thereby displaying the hexagonal bipyramid. As pointed out by Doye and Wales,[13] Pb_{15} is one of the Frank–Kasper coordination polyhedra[7,35] and is the global minimum for a long-ranged Morse potential.[36]

(2) The cluster sizes Pb_{16}–Pb_{20} mark the beginning of the cluster formation of Pb where there is a tendency for the development of clusters not falling neatly into any of the ordered morphologies. Growth pattern for these five clusters can be classified as distorted decahedra. The Pb_{16} is formed by capping atoms on three of the five-square faces in the 13-atom Ino decahedron. However, these capped atoms are distorted, occupying sites as close as possible. The clusters Pb_{17}–Pb_{20} develop by capping one atom at a time the available square faces. Similar distorted decahedra were predicted for the Sutton–Chen 10-8 potential.[13]

(3) Turning to clusters Pb_{21}–Pb_{56}, the cluster formation follows a very different pattern from that seen for the alkali

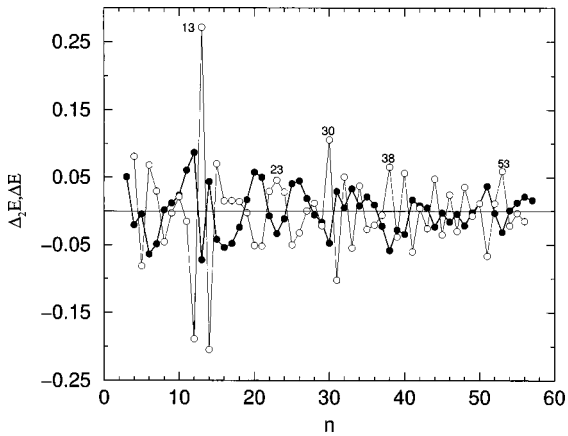

FIG. 5. The energy difference $\Delta E(n)$, denoted by closed circles, and the second energy difference $\Delta_2 E(n)$, denoted by open circles, for the metallic clusters Pb.

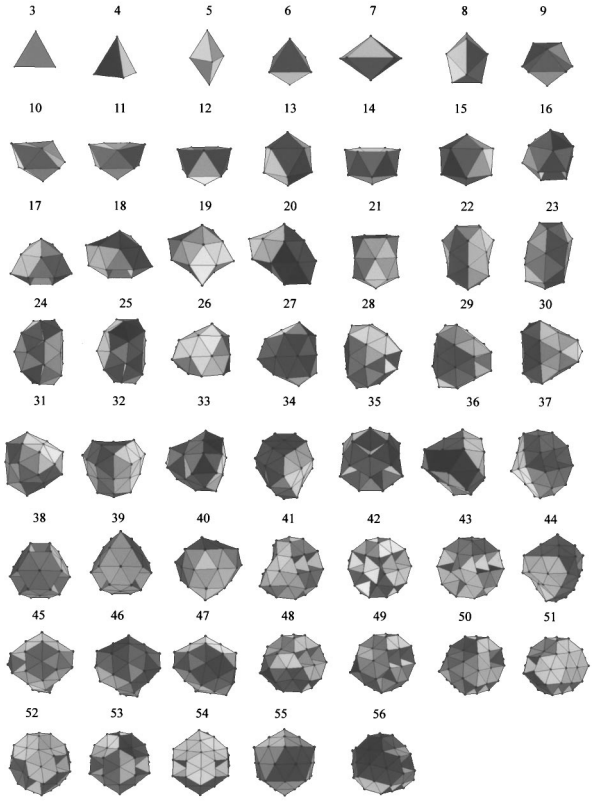

FIG. 6. Structures of the global energy minima for the metallic clusters Pb calculated using Eqs. (1)–(3) with parameters documented in Table I. Within the accuracy of the energies presented here, the genetic algorithm and the basin hopping methods yield the same results.

metals. The Pb_{21}, for example, is formed when six atoms are added to the faces surrounding a vertex in Pb_{14}. Proceeding from Pb_{22}, the structures generally have lower symmetry, and the ground-state geometries of many clusters resemble those of the Sutten–Chen 10-8 potential (or the Sutten–Chen 9-6 potential for Pb_{28}, Pb_{31}, Pb_{32}, and Pb_{44})[13] at their respective global minima. It can be seen that many of the disordered structures found in this work have surface structure of an incomplete Mackay icosahedron. However, the structures are, in one way or another, distorted. We check further that the structures for Pb_{22}, Pb_{24}, Pb_{25}, Pb_{29}, Pb_{30}, $Pb_{37}-Pb_{39}$, Pb_{42}, Pb_{45}, Pb_{52}, and Pb_{53} are identical to those for the Sutten–Chen 10-8 potential reported by Doye and Wales.[13] The atomic distributions described in their work for these clusters are therefore equally applicable here. Perhaps we should mention further two closely connected sequences. The first sequence begins with Pb_{36} which leads to Pb_{44} with the addition of eight atoms in which three of them occupy sites that, together one atom existing there, form a distorted rhombus. For the remaining five atoms, we find four atoms forming a planar rhombus face (see the bottom four atoms) and the last atom locating at a site of a distorted hexagonal face. Similar analysis can be applied to understand the development of clusters $Pb_{45}-Pb_{47}$, although it becomes more complex in going to Pb_{47}. The second sequence starts with Pb_{37} which develops into Pb_{42} by removing one apex atom of a pentagonal pyramid and placing the latter at the apex site of one of two newly formed pentagonal pyramids whose sites are where the five additional atoms locate. In arriving at Pb_{42}, the original apex-missing pentagonal pyramid is slightly distorted, however. Then, Pb_{43} is formed by occupying this missing apex again. Away from Pb_{43}, the cluster growth continues with Pb_{48} where the apex atom mentioned in Pb_{43} together with five additional ones establish a new pentagonal pyramid. From hereon one can easily trace the cluster growth pattern by the addition of one atom at a time to the preceding Pb_n. Apart from these sequences, the cases of Pb_{38} and Pb_{55} are also of interest. The former assumes the same close-packed structure as the K_{38}, Pb_{38}, and the three Sutton–Chen potentials given in the work of Doye and Wales,[13] whereas in the latter, according to Fig. 5, the energy difference at $n=55$ does not indicate a stable global minimum cluster. However, as in alkali metallic clusters, Pb_{55} reveals the 55-atom Mackay icosahedron. In brief, we have found the structural growth pattern of Pb clusters to evolve with a tendency and preference for forming close-packed or decahedral clusters dramatically different from the icosahedral preference seen for alkali metals.

IV. SUMMARY AND CONCLUSION

We study the ground-state structures of metallic clusters Na, K, Rb, Cs, and Pb in the size range $3 \leqslant n \leqslant 56$. The analytical Gupta-type many-body potential is applied to account for the many-body interactions between atoms. Both the genetic algorithm technique and the basin hopping method have been used to locate the global energy minima of clusters. For four monovalent and a polyvalent metals studied in this work, we find that the global energy minima predicted by the basin hopping method are the same as those obtained from the genetic algorithm, thus ensuring the optimization values predicted. For the equilibrium energy of alkali metallic clusters at $T=0$ K, our calculations for the $\Delta E(n)$ and $\Delta_2 E(n)$ show regularities in cluster stability, but the general characteristics are quite different from those displayed for the tetravalent lead clusters. Specifically, the Pb metallic clusters have the tendency of distributing atoms at sites formed by intervening the pentagonal and hexagonal pyramids. The morphology is such that the pyramids, generally distorted, interlock with three shared atoms one of which is the apex of the other pyramid. The close-packed and decahedral patterns are thus prominent features for the morphology of Pb clusters, a finding in agreement with the theoretical studies of Lim *et al.*,[37] who showed by molecular dynamics simulation for the binding energies of Pb_n, $n \geqslant 55$, that nonicosahedral minima are more energetically favorable than the icosahedral minima. We should finally make a comment on the cluster $\mathfrak{I}_{13}$. This extremely stable cluster is predicted for all of the sp-type metallic clusters considered here as well as for transition/noble/alkali earth metals,[38–40] Lennard-Jones potential,[41] $(C_{60})_N$,[42] Sutton–Chen potential,[13] and Morse potential.[36] Accordingly, it would thus appear that the previous molecular dynamics simulation study of the liquid–glass transition[43] attributing the 13-atom icosahedron as stable units in the glass formation is not unreasonable from the point of view of the cluster growth found here.[44]

ACKNOWLEDGMENTS

This work has been supported in part by the National Science Council (NSC89-2112-M-008-049), and the NSERC of Canada. S.K.L. would like to express his gratitude to the Department of Physics at the University of Waterloo for its hospitality during a visit, and is thankful to Professor Y. Okabe for hosting his visit to the Department of Physics at the Tokyo Metropolitan University where the final stage of the paper was written to fruition. We acknowledge continual support from the National Central University.

[1] C. L. Cleveland and U. Landman, J. Chem. Phys. **94**, 7376 (1991).
[2] O. D. Häberlen, S. C. Chung, M. Stener, and N. Rösch, J. Phys. Chem. B **106**, 5189 (1997).
[3] C. L. Cleveland, U. Landman, T. G. Schaaff, M. N. Shafigullin, P. W. Stephens, and R. L. Whetten, Phys. Rev. Lett. **79**, 1873 (1997).
[4] F. Calvo and F. Spiegelmann, J. Chem. Phys. **112**, 2888 (2000).
[5] N. Ju and A. Bulgac, Phys. Rev. B **48**, 2721 (1993).
[6] R. S. Berry and B. M. Smirnov, J. Chem. Phys. **113**, 728 (2000).
[7] J. P. K. Doye and D. J. Wales, J. Phys. B **29**, 4859 (1996).
[8] J. P. K. Doye and F. Calvo, J. Chem. Phys. **116**, 8307 (2002).
[9] T. P. Martin, T. Bergmann, H. Göhlich, and T. Lange, Chem. Phys. Lett. **172**, 209 (1990).
[10] H. Hubert, B. Devouard, L. A. J. Garvie, M. O'Keeffe, P. R. Buseck, W. T. Petuskey, and P. F. McMillan, Nature (London) **391**, 376 (1998).
[11] Y. Zeiri, Phys. Rev. E **51**, R2769 (1995).
[12] J. A. Niesse and H. R. Mayne, J. Chem. Phys. **105**, 4700 (1996).
[13] J. P. K. Doye and D. J. Wales, New J. Chem. **22**, 733 (1998).
[14] R. P. Gupta, Phys. Rev. B **23**, 6265 (1981).
[15] F. Ducastelle, J. Phys. (Paris) **31**, 1055 (1970).
[16] J. Friedel, in *Electrons, Physics of Metals*, Vol. I, edited by J. M. Ziman (Pergamon, London, 1969).
[17] F. Cleri and V. Rosato, Phys. Rev. B **48**, 22 (1993).
[18] Y. Li, E. Blaisten-Barojas, and D. A. Papaconstantopoulos, Phys. Rev. B **57**, 15519 (1998). For sodium, the Gupta potential parameters were taken from the work by the same authors in Chem. Phys. Lett. **268**, 331 (1997).
[19] The interested readers may consult the early work of Cleri and Rosato (Ref. 17) and a more recent one of Chien *et al.* (Ref. 38) for details.
[20] W. Y. Ching and J. Callaway, Phys. Rev. B **11**, 1324 (1975).
[21] G. Allan and M. Lanoo, Phys. Status Solidi B **74**, 409 (1976).
[22] W. Zhong, Y. S. Li, and D. Tomanek, Phys. Rev. B **44**, 13 053 (1991).
[23] M. M. Sigalas and D. A. Papaconstantopoulos, Phys. Rev. B **49**, 1574 (1994).
[24] N. A. Besley, R. L. Johnson, A. J. Stace, and J. Uppenbrink, J. Mol. Struct.: THEOCHEM **34**, 75 (1995).
[25] D. Liu and J. Nocedal, Math. Program. B **45**, 503 (1989).
[26] J. A. Niesse and H. R. Mayne, Chem. Phys. Lett. **261**, 576 (1996).
[27] Y. Zeiri, Comput. Phys. Commun. **103**, 28 (1997).
[28] D. J. Wales and J. P. K. Doye, J. Phys. Chem. A **101**, 5111 (1997).
[29] Z. Li and H. A. Scheraga, Proc. Natl. Acad. Sci. U.S.A. **84**, 6611 (1987).
[30] W. D. Knight, K. Clemenger, W. A. de Heer, W. A. Saunders, M. Y. Chou, and M. L. Cohen, Phys. Rev. Lett. **52**, 2141 (1984).
[31] A. Aguado, J. M. Lopez, J. A. Alonso, and M. J. Stott, J. Chem. Phys. **111**, 6026 (1999).
[32] U. Röthlisberger and W. Andreoni, J. Chem. Phys. **94**, 8129 (1991).
[33] V. Bonacic-Koutecky, P. Fantucci, and J. Koutecky, Phys. Rev. B **37**, 4369 (1988).
[34] F. Spiegelmann and D. Pavolini, J. Chem. Phys. **89**, 4954 (1988).
[35] F. C. Frank and J. S. Kasper, Acta Crystallogr. **11**, 184 (1958); **12**, 483 (1959).
[36] J. P. K. Doye and D. J. Wales, J. Chem. Soc., Faraday Trans. **93**, 4233 (1997).
[37] H. S. Lim, C. K. Ong, and F. Ercolessi, Surf. Sci. **269/270**, 1109 (1992).
[38] C. H. Chien, E. Blaisten-Barojas, and M. R. Pederson, J. Chem. Phys. **112**, 2301 (2001).
[39] S. Darby, T. V. Mortimer-Jones, R. L. Johnston, and C. Roberts, J. Chem. Phys. **116**, 1536 (2002).
[40] J. E. Heam and R. L. Johnston, J. Chem. Phys. **107**, 4674 (1997).
[41] J. A. Northby, J. Chem. Phys. **87**, 6166 (1987).
[42] Y. H. Luo, J. Zhao, S. Qiu, and G. Wang, Phys. Rev. B **59**, 14903 (1999).
[43] F. Yonezawa, S. Nose, and S. Sakamoto, Z. Phys. Chem. (Leipzig) **156**, 5451 (1988).
[44] We exclude the network glassy materials such as the Si or Ge where directional terms in the many-body potential must be explicitly included. This class of clusters therefore differs from the ones mentioned here.